Pore Characteristics for Efficient CO_2 Storage in Hydrated Carbons

Muqing Ren,[†] Marta Sevilla,[≠] Antonio B. Fuertes,[≠] Robert Mokaya,[#,] James M. Tour[†,‡,§,*] and Almaz S. Jalilov[¶,*]*

[†]Department of Chemistry, [‡]The NanoCarbon Center, [§]Department of Materials Science and NanoEngineering,

Rice University, 6100 Main Street, Houston, Texas 77005, USA

[¶]Department of Chemistry and Center for Integrative Petroleum Research, King Fahd University of Petroleum and Minerals, Dhahran, Saudi Arabia 31261

[#]School of Chemistry, University of Nottingham. University Park, Nottingham NG7 2RD, United Kingdom

[≠]Instituto Nacional del Carbon (CSIC), Francisco Pintado Fe 26, Oviedo 33011, Spain

**Email: r.mokaya@nottingham.ac.uk, tour@rice.edu, jalilov@kfupm.edu.sa*

ABSTRACT Development of new approaches for carbon dioxide (CO_2) capture is important in both scientific and technological aspects. One of the emerging methods in CO_2 capture research is based on the use of gas-hydrate crystallization in confined porous media. Pore dimensions and surface functionality of the pores play important roles in the efficiency of CO_2 capture. In this report, we summarize work on several porous carbons (PCs) that differ in pore dimensions that range from supermicropores to mesopores, as well as surfaces ranging from hydrophilic to hydrophobic. Water was imbibed into the PCs and the CO_2 uptake performance, in dry and

hydrated forms, was determined at pressures of up to 54 bar to reveal the influence of pore characteristics on the efficiency of CO_2 capture and storage. The final hydrated carbon materials had H_2O to carbon weight ratios of 1.5:1. Upon CO_2 capture, the H_2O/CO_2 molar ratio was found to be as low as 1.8, which indicates a far greater CO_2 capture capacity in hydrated PCs than ordinarily seen in CO_2−hydrate formations, wherein the H_2O/CO_2 ratio is 5.72. Our mechanistic proposal for attainment of such a low H_2O/CO_2 ratio within the PCs is based on the finding that most of the CO_2 is captured in gaseous form within micropores of diameter < 2 nm, wherein it is blocked by external CO_2-hydrate formations generated in the larger mesopores. Therefore, in order to have efficient high pressure CO_2 capture by this mechanism, it is necessary to have PCs with a wide pore size distribution consisting of both micropores and mesopores. Furthermore, we found that hydrated microporous or supermicroporous PCs do not show any hysteretic CO_2 uptake behavior, which indicates that CO_2–hydrates cannot be formed within micropores of diameter 1-2 nm. Alternatively, mesoporous and macroporous carbons can accommodate higher yields of CO_2-hydrates, which potentially limits the CO_2 uptake capacity in those larger pores to a H_2O/CO_2 ratio of 5.72. We found that high nitrogen content prevents the formation of CO_2-hydrates presumably due to their destabilization and associated increase in system entropy *via* stronger noncovalent interactions between the nitrogen functional groups and H_2O or CO_2.

Keywords: Carbon dioxide capture, porous carbons, carbon nanotechnology, gas hydrates, absorption, mechanism, pore size.

INTRODUCTION

Porous materials are important for the capture, separation and conversion of greenhouse gases such as carbon dioxide (CO_2).[1-3] Among the many existing classes of porous materials, porous carbons (PCs) have received a great deal of attention as adsorbents due to their attractive physical and chemical properties and stability.[4,5] In particular, the prospect of designing PCs with well-defined porosity within the range of supermicroporosity to macroporosity is currently attracting much research effort for potential applications in catalysis, energy storage, gas separations and for environmental remediation and conservation.[6-9] Additionally, the development of PCs with precise pore dimensions within the sub-nanometer range that can rival porous materials such as zeolites or metal-organic frameworks is of interest.[10,11] Particularly important are micropores and supermicropores, which are relevant to any efforts to physically and selectively trap CO_2 *via* molecular sieving approaches. Such capture of CO_2 requires narrow pores that are close to the kinetic diameter of molecular CO_2, *i.e.*, 0.33 nm.[12,13] The molecular sieving approach is especially important for post-combustion CO_2 capture technologies that require lower CO_2 adsorption enthalpy and faster kinetics for release of the CO_2. Alternatively, larger diameter mesoporous and macroporous carbons have been shown to be amenable to surface modifications that act to enhance CO_2 capture capacity and selectivity *via* increased CO_2 adsorption enthalpy.[14-16] Therefore, various surface modification techniques, such as heteroatom doping to increase Lewis basic sites,[17-19] surface oxidation to increase the polarity,[20,21] as well as noncovalent doping using polymeric amines,[15] are an important part of recent research toward development of CO_2 capture technology. Introducing traces of water within porous media has been shown to greatly enhance CO_2 capture efficiency *via* the formation of CO_2 gas hydrates.[22-24]

Gas-hydrates are crystalline host-guest compounds consisting of ordered hydrogen-bonded porous water clusters that contain gas molecules in a void cavity.[25-28] A dodecahedral water cluster with CO_2 inside the cavity is shown in Figure 1. The stability of gas-hydrates depends on the strength of the noncovalent interactions between the host water molecules and the guest molecules. Hence, their stability differs significantly upon changing the guest molecules, which can be CO_2, nitrogen (N_2), methane (CH_4), hydrogen sulfide (H_2S) or other gases.[29,30] Therefore, apart from CO_2 capture technologies that are based on the kinetic diameter of CO_2 and strong noncovalent interactions of CO_2 with amines, the gas-hydrate based CO_2 capture processes gives an added dimension for tuning the CO_2 capture capacity and selectivity of porous materials.[31]

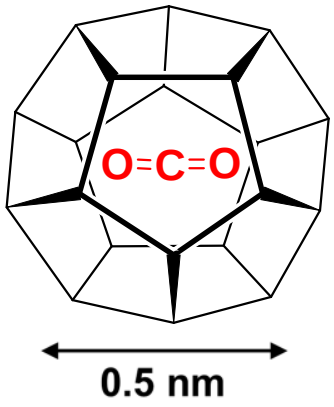

Figure 1. Schematic representation of CO_2 hydrates consisting of dodecahedral water clusters with CO_2 trapped inside the cavity.

Gas-hydrates have been effectively employed for methane storage and transportation.[32] CO_2 capture technology using hydrate-based processes is increasingly being explored although the mechanism for adsorption is not well elucidated.[33] Various materials such as porous aluminium,[34] activated carbons,[35,36] silica,[37] as well as metal-organic frameworks,[38,39] have been employed for hydrate-based CO_2 capture processes. In general, there are three forms of gas-hydrate structures,

which are denoted as structure I, structure II and structure H.[40] All three structures have been identified and investigated using X-ray diffraction studies.[40] These three forms differ in the size of their crystallographic unit cell, cavity types, water content and types of gas molecules that they can host within their cavities. CO_2 mainly exists in CO_2–hydrates in the form of structure I, which has a unit cell of a 1.2 nm cube with 46 molecules of water and two types of cavities. Structure II has larger amounts of water molecules, and therefore has larger unit cell dimensions. Structure H is the least stable, and has the smallest unit cell dimensions, with three different types of cavities that can host various size molecules such as methane and larger chain hydrocarbons.[41] In confined porous media, particularly when the pore diameters approach the sizes of the unit cell of gas–hydrates, the properties and stability of the gas–hydrates are expected to change and approach the limits of geometrical restrictions governed by the porous structure.

Herein, we report the CO_2 capture characteristics of hydrated PCs that differ in their pore size distribution and surface functionalities. To explore the effect of pore size distribution on CO_2 uptake, we accordingly selected PCs with diameters ranging from the microporous/supermicroporous regime to predominantly mesoporous. This work builds on our recent preliminary report on gas-hydrate-based CO_2 storage in porous carbon materials,[42] but, *via* a series of carefully selected samples and experiments, goes much further in more clearly elucidating the effect of the pore dimensions, elemental composition and surface functionalities. By exploring the CO_2 uptake performance of several PCs in their dry and hydrated forms, we are able to discuss mechanistic details and the role of pore dimensions and surface functionalities on high-pressure CO_2 storage *via* CO_2-hydrate formation.

RESULTS AND DISCUSSION

Micro-/Mesoporous Carbon Characterization. PCs were selected that have pore size distribution within different size ranges, namely, narrow distribution of ultra-microporosity, mixed pore size distributions within micro-and mesoporosity, and predominantly mesoporous. Details of sample preparation procedures and associated characterization data, including analysis for morphology of the PCs have been previously reported.[9, 42-45] Herein, we report on selected and additional data on the pore structure, surface composition and elemental composition of the PCs, which are relevant to the hydrate-based CO_2 capture process. Details of pore structure, such as porosity, Brunauer–Emmett–Teller (BET) surface area, pore volume, relative content of microporosity and the pore size distribution (PSD) of the PCs were analyzed by means of nitrogen sorption (at 77 K), and the isotherms are shown in Figure 2, while the corresponding PSDs are shown in Figure 3. As seen from Figure 2, both samples G-800 and G-850-5 exhibit Type I isotherm, with the major adsorption at low relative pressures, *i.e.*, < 0.05, which is characteristic of microporous adsorbents.[46] The isotherm of sample G-2.3-2 shows some deviation from Type I, and indicates the presence of some mesopores. The PSDs in Figure 3 reveal that sample G-2.3-2 has some pores of size >2 nm, while on the other hand, both sample G-800 and G-850-5 do not exhibit any pores of size > 2 nm. This is a significant observation in the context of the present study especially given that, despite the differences in their PSD, samples G-800, G-850-5 and G-2.3-2 have comparable surface area (Table 1).

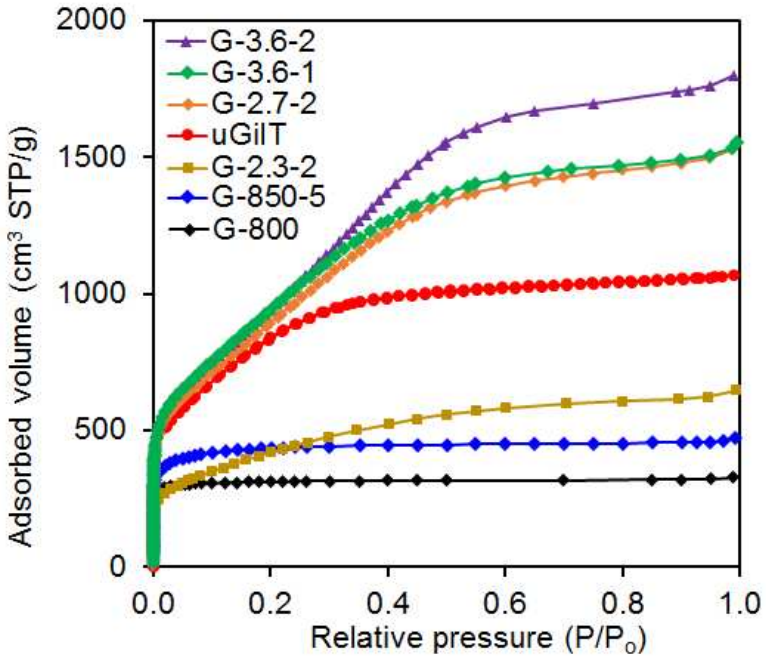

Figure 2. Nitrogen sorption isotherms of porous carbons at 77 K.

Table 1. Textural properties of porous carbons

Sample	Textural properties			Chemical composition [at. %]				XPS [at. %]		
	S_{BET} [m^2 g^{-1}]	V_p [cm^3 g^{-1}][a]	V_{micro} [cm^3 g^{-1}][b]	H	C	N	O	C	N	O
G-2.7-2	3310	2.36	1.00 (42)	0.7	90.1	3.8	5.4	86.7	5.8	7.5
G-2.3-2	1520	0.96	0.52 (54)	1.5	73.5	15.4	9.6	80.3	15.7	4.0
G-3.6-2	3460	2.72	1.00 (37)	0.4	92.5	2.7	4.4	95.0	1.0	4.0
G-3.6-1	3470	2.37	1.10 (46)	0.4	94.4	1.0	4.2	91.3	3.8	4.9
G-850-5	1690	0.71	0.64 (90)	-	-	-	-	97.2	1.3	1.5
G-800	1270	0.50	0.46 (92)	-	-	-	-	91.5	<0.1	8.5
uGilT	2860	1.65	1.21 (73)	-	-	-	-	93.4	<0.1	6.6

[a]Total pore volume was determined at a P/P_o of ~0.95. [b]Micropore volume was determined using the the QSDFT PSD. The percentage of pore volume that arises from micropores is given in parentheses.

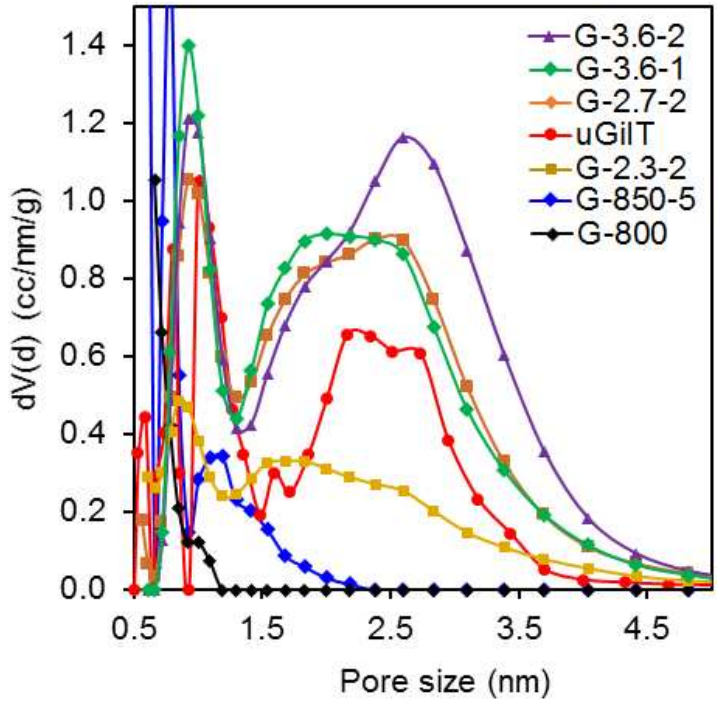

Figure 3. Pore size distribution curves of the PCs.

On the other extreme, with respect to microporosity, are samples G-2.7-2, G-3.6-1 and G-3.6-2, which are predominantly mesoporous and have the highest BET surface area in the range 3310–3470 $m^2\ g^{-1}$ and pore volume of 2.36–2.72 $cm^3\ g^{-1}$. These samples also exhibit the lowest proportion of micropores (≤46 %) and the highest content of mesopores of size >2 nm as shown in Figures 2 and 3. The mesopore-rich PCs (G-2.7-2, G-3.6-1 and G-3.6-2) show type-IV isotherms that are typical of mesoporous adsorbents. The final sample in this study is uGilT, which represents a porous carbon with a mixture of microporous and mesoporous characteristics, along with high BET surface area of 2860 $m^2\ g^{-1}$ and pore volume of 1.65 $cm^3\ g^{-1}$. uGilT has 73% of micropore

volume (Table 1). The nitrogen sorption isotherm for uGilT is intermediate between type I and IV, and the sample exhibits the narrowest mesopore size distribution (centered at ca. 2.5 nm) of all the studied materials (Figure 2 and 3).

The surface characteristics of the PCs were studied by means of X-ray photoelectron spectroscopy (XPS). Table 1 summarizes the elemental composition of the PCs as estimated using two different methods, bulk elemental analysis and XPS analysis. While bulk elemental analysis is better at quantitative determination of the composition of the bulk materials, XPS analysis more accurately captures the composition of the surface and near surface region of the PCs. Elemental analysis data of G-2.7-2 and G-3.6-1 show higher amounts of carbon and lower oxygen content compared to the corresponding XPS data. This suggests that the surface and near surface region of samples G-2.7-2 and G-3.6-1 have higher oxygen content compared to the bulk. Overall, high resolution XPS analysis revealed a broad range of oxygen content on the surface of the PCs. Sample G-850-5 has the lowest oxygen content of 1.5%, which makes it the most hydrophobic of all studied PCs. The other samples have oxygen content in the range of 4.0 – 8.5%; we have previously shown that the oxygen content of carbon materials can vary between 1.8% for superhydrophobic surfaces, to 15% for superhydrophilic surfaces.[47] Sample G-800 has the highest oxygen content and is therefore expected to be the most hydrophilic, with a C/O ratio of 9.5. In comparison, sample G-850-5 has C/O ratio of 37.5 (Table 2) and is expected to be hydrophobic. We highlight the O content and hydrophilicity or hydrophobicity of these two samples (G-850-5 and G-800) as they have comparable pore structure and surface area. Deconvoluted peaks of high resolution XPS spectra (C 1s and O 1s) of the PCs are shown in Figure 4. The deconvoluted C 1s peaks (Table 2) reveal that graphitic carbon (C─C/C=C) with peak at 284.8 eV is the main component for all the PCs. (Note that the all of the spectra were centered at 284.8 eV for the

graphitic carbon in order to calibrate other peak positions). The oxygen-containing groups in all PCs are predominantly in the form of ether, epoxy and hydroxyl (C─O, C─O─C, and C─OH, 286.2 eV) groups. Carbonyl (C=O, 287.4 eV) groups are also present in the form of ketones or quinones and carboxyl (HO─C=O, 289.0 eV) groups, as shown in Suporting Information Figures S1-S7. The relative contributions of each functional group are summarized in Table 2.

Table 2. Elemental composition of porous carbons estimated from the C 1s and O1s peaks of high resolution XPS.

Sample	C/O	C 1s [%]						O 1s (%)	
		C–C/C=C	C–O	C=O	N–C=O	O–C=O	π-π*	C=O	C–O
G-2.7-2	11.6	65.28	15.75	7.3	4.85	3.05	3.77	23.66	76.34
G-2.3-2	22.4	61.44	18.34	8.76	5.39	2.8	3.26	42.53	57.47
G-3.6-2	21.3	65.86	16.07	6.59	4.47	2.91	4.1	21.37	78.63
G-3.6-1	17.5	67.36	15.95	6.01	4.27	2.75	3.66	14.49	85.51
G-850-5	37.5	79.88	17.29	2.12	0.71	0	0	56.2	43.8
G-800	9.5	74.66	10.85	6.33	3.84	2.7	1.62	29.76	70.24
uGilT	14.2	73.64	13.53	5.66	3.28	2.24	1.65	33.21	66.79

To further evaluate the oxygen functionalities of the PCs, we deconvoluted the O 1s peaks as shown in Figure 4. The O 1s spectra was deconvoluted into two main peaks; carbonyl-carboxyl (C=O and $^{-}$O─C=O, ~531.6 eV) groups and the hydroxyl-ether (C─O and C─O─C, ~533.1 eV) groups. Relative contributions of each oxygen functional groups are summarized in Table 2. In general, the PCs show higher content of C─O groups, except for G-850-5, which has higher

proportion of C=O groups and the lowest oxygen content. It is also noteworthy that G-2.3-2 and G-2.7-2 have higher content of nitrogen functionalities (Table 1). The N 1s spectra for both were deconvoluted into two main peaks, with binding energies at ~398.5 and ~401.1 eV, and which correspond to pyridinic N and pyrrolic N-bonding configurations, respectively (Figures S8 and S9). The effect of each surface bonding configuration in combination with the pore structure were further evaluated with respect to the CO_2-sorption properties of the hydrated PCs.

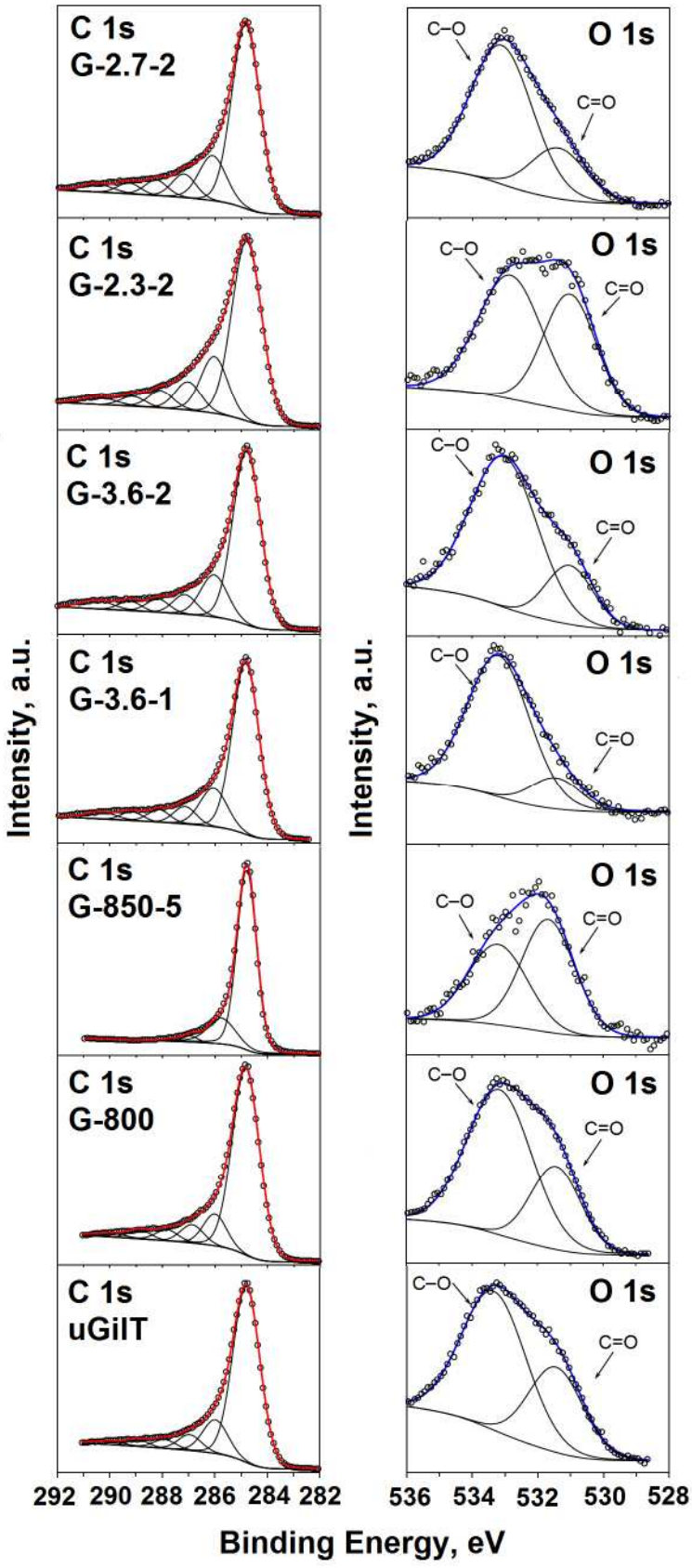
C 1s
G-2.7-2
C 1s
G-2.3-2
C 1s
G-3.6-2
C 1s
G-3.6-1
C 1s
G-850-5
C 1s
G-800
C 1s
uGilT
O 1s
C–O
C=O
Intensity, a.u.
292 290 288 286 284 282
536 534 532 530 528
Binding Energy, eV

Figure 4. C 1s and O 1s X-ray photoelectron spectra of PCs.

CO_2–Uptake Characteristics of the Hydrated Micro-/Mesoporous Carbons. Water containing (*i.e.*, hydrated) PCs were prepared as previously reported.[42] The hydrated PCs were prepared to a target water content of 150 wt%, and are hereinafter denoted as PC(H_2O) (see Experimental Section for details). It is also noteworthy to mention that upon hydration of PCs BET surface area drastically decrease, revealing the enrichment of the pores by water.[42] The gravimetric CO_2 uptake isotherms for G-800 and G-800(H_2O), uGilT and uGilT(H_2O) and G-3.6-1 and G-3.6-1(H_2O) at 25 °C and pressure of up to 54 bar are shown in Figure 5. As expected, dry G-800 has a CO_2 uptake isotherm that is typical for a microporous material with sharp uptake at low pressure (<5 bar) and thereafter tending towards saturation at pressures above 10 bar. In contrast, both uGilT and G-3.6-1 exhibit a gradual, almost linear, increase in CO_2 uptake due to filling of mesopores as pressure increases up to ~ 40 bar, followed by a more gradual rise to the final pressure of 54 bar. The higher CO_2 uptake capacity of G-3.6-1 compared to uGilT correlates with the higher BET surface area of the former. However, the CO_2-uptake isotherms for the hydrated PCs, G-800(H_2O), uGilT(H_2O) and G-3.6-1(H_2O) reveal that each of the samples exhibits a unique relationship between pore structure and the CO_2 uptake (the uptake is defined with respect to the mass of the carbon). We have previously shown that sample uGilT(H_2O) shows an S-shaped CO_2 sorption isotherm, with low uptake at pressures of up to 20 bar, after which the uptake drastically rises from 4.6 to 30 mmol g^{-1} (20 to 132 wt%) as pressure increases from 20 to 40 bar.[42] The desorption of CO_2 reveals clear hysteretic behavior for the CO_2 sorption isotherm of uGilT(H_2O), which rejoins the adsorption branch at 15 bar. Complete release of the CO_2 is attained at ~ 1 bar. The hysteresis width for uGilT(H_2O) is ~6 bar. Comparison of the CO_2 sorption isotherm for dry uGilT to that of hydrated uGilT(H_2O) indicates that the total CO_2 uptake capacity (at pressure of 54 bar) is similar

for both samples at 30 mmol g^{-1}. It is important to note that uGilT has a micropore volume content of 73% with the remainder of pore volume presumably arising from mesopores. Using *in situ* IR-spectroscopy, we have previously shown that hysteretic behavior of the CO_2–sorption isotherm is due to the formation of CO_2–hydrates that start to form at ~ 20 bar in the confined pore spaces of uGilT(H_2O).[42] It is important to compare the CO_2 uptake isotherm of uGilT(H_2O) with that of the supermicroporous G-800(H_2O) sample that has micropore volume content of 92%. Unlike uGilT(H_2O), sample G-800(H_2O) does not exhibit any hysteretic S-shaped CO_2 sorption isotherm behavior (Figure 5) for pressures up to the critical point of CO_2 at 54 bar. Rather, G-800(H_2O) shows only a gradual increase in uptake that reaches 5.5 mmol g^{-1} at 54 bar, behavior that resembles that of macroporous materials. This behavior could be explained by considering that the micropores of the hydrated G-800(H_2O) are filled with water molecules, which prevents the formation of CO_2-hydrates within the small pores.[48-50] The small gradual increase in the CO_2 uptake capacity as pressure increases may be ascribed to the filling of residual macropores. As mentioned above, the single unit cell of the gas-hydrates have lengths of 1.2 nm and, therefore it is necessary to have pores larger than 1.2 nm for efficient formation of the gas-hydrates. Contrarily, sample G-3.6-1(H_2O) reveals a hysteretic CO_2 sorption isotherm that is similar to that of uGilT(H_2O), except that the step of rapid increase in CO_2 uptake takes place at higher pressure range of between 30 and 50 bar (compared to 20 to 40 bar for uGilT(H_2O)), and that the desorption branch rejoins the adsorption branch at 25 bar (compared to 15 bar for uGilT(H_2O)). G-3.6-1(H_2O) also shows wider hysteresis width of 12.3 bar. Sample G-3.6-1 has higher surface area than uGilT and higher CO_2 uptake capacity, and it might be expected that hydrated G-3.6-1(H_2O) would have higher CO_2-sorption capacity compared to hydrated uGilT(H_2O) at the maximal pressure of 54 bar. The fact that these two samples (G-3.6-1(H_2O) and uGilT(H_2O)) have similar CO_2 uptake

capacity at 54 bar points to the higher concentration and extent of CO_2-hydrate formation within G-3.6-1(H_2O) in comparison to uGilT(H_2O). This explanation is consistent with the wider hysteresis width for G-3.6-1(H_2O) in comparison to uGilT(H_2O). Wider hysteresis width would suggest higher stability of the CO_2-hydrates. Moreover, *in situ* IR-spectroscopy reveal the direct evidence for the CO_2-hydrate formation in both G-3.6-1(H_2O) and uGilT(H_2O), unlike G-800(H_2O) that does not show an increase in H_2O stretching peaks, as shown in Figure 5b.[42]

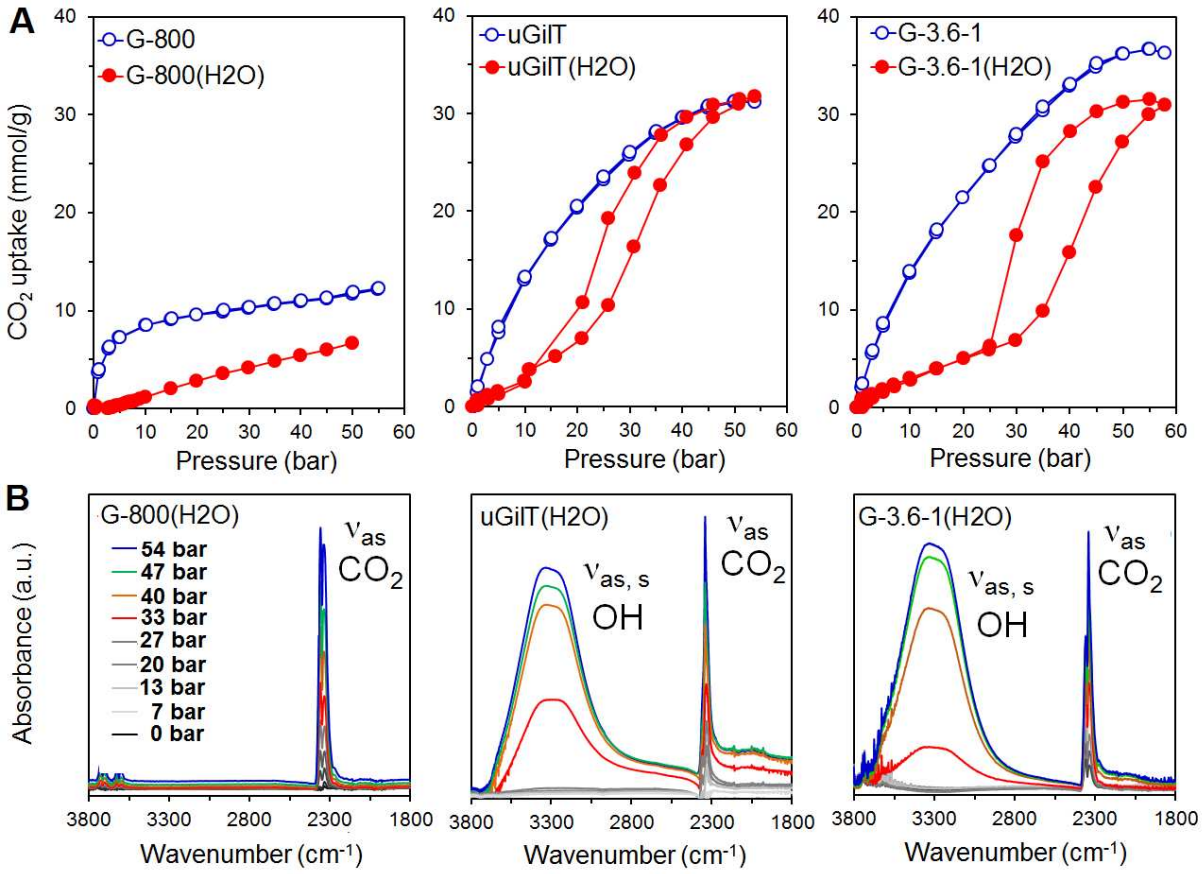

Figure 5. A) Comparison of the CO_2 sorption isotherms for dry G-800, uGilT and G-3.6-1 (blue, open circles) and hydrated G-800(H_2O), uGilT(H_2O) and G-3.6-1(H_2O) (red filled circles) at 25 ^oC. B) ATR-IR absorption spectra of hydrated G-800(H_2O), uGilT(H_2O) and G-3.6-1(H_2O) as a

function of CO_2 pressure. The CO_2 uptake measurements were performed using a gravimetric gas uptake apparatus, and the carbons had H_2O content of ~150 wt%.

In addition to the microporous G-800(H_2O), we also tested sample G-850-5(H_2O) for CO_2-storage performance (Figure 6a). The only distinction between the G-800(H_2O) and G-850-5(H_2O) is that G-800 has the highest content of oxygen functionalities while G-850-5 has the lowest. Therefore, G-850-5 is expected to be the most hydrophobic. The higher hydrophobicity could be the reason for the lower CO_2 sorption capacity of G-850-5(H_2O) as shown in Figure 6a. For further comparison, Figure 6a also shows the CO_2 uptake performance of G-2.3-2(H_2O) at 25 °C. Interestingly, the relatively more mesoporous G-2.3-2(H_2O) sample has CO_2 uptake behavior that is similar to that of the more microporous samples (Figure 6a). This is despite the fact that sample G-2.3-2 has lower microporosity (54%) compared to G-850 (92%), G-850-5 (90%) and even uGiT (73%). It is clearly evident, and indeed surprising, from Figure 6a, that G-2.3-2(H_2O) along with G-800(H_2O) and G-850-5(H_2O) do not show any hysteretic properties for CO_2 sorption. In seeking to explain the anomalous behavior of G-2.3-2(H_2O), it is also noteworthy to consider that sample G-2.3-2 has the highest content of nitrogen among all the PCs at 15.7% (Table 1). The lack of an S-shape CO_2–sorption isotherm for the significantly mesoporous G-2.3-2(H_2O) sample implies that surface nitrogen functionalities, which can generate Lewis basic sites, act to prevent the formation of CO_2-hydrates. Destabilization of CO_2-hydrates in the presence of nitrogen functionalities could arise due to increased basicity, which would engender stronger interactions between the nitrogen containing sites and CO_2 or H_2O. The overall effect would be that the nitrogen functional groups act to increase the system entropy by increasing the disorder of the water molecules. However, we note that further details and understanding of the effect of other

surface functional groups on gas-hydrate formations within porous media is crucial, but beyond the scope of this work, which is primarily focused on the influence of pore structure.

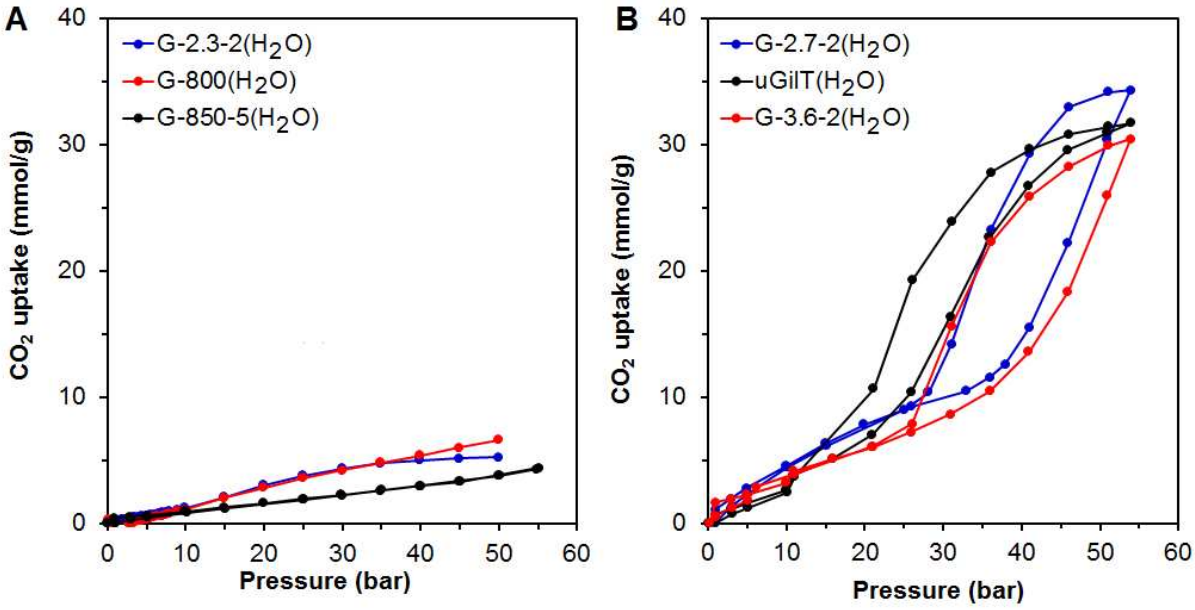

Figure 6. Comparison of the CO_2 sorption isotherms for various hydrated porous carbons A) without CO_2-hydrate formation and B) with CO_2-hydrate formation at 25 ºC. The CO_2 uptake measurements were performed using a gravimetric gas uptake apparatus, and the carbons had H_2O content of ~150 wt%.

Figure 6b summarizes the CO_2–sorption performance of mesoporous G-2.7-2(H_2O) and G-3.6-2(H_2O), and includes uGilT(H_2O) for comparison. Both samples G-2.7-2(H_2O) and G-3.6-2(H_2O) show a behavior that is similar to that of uGilT(H_2O), except that the hysteresis curve is shifted to higher pressures. The other feature of the CO_2 sorption on hydrated PCs that was explored is the sample to sample variation in the hysteresis width, and its relationship with the proportion of microporosity. Figure 7 plots the relationship between micropore % and the

hysteresis width (bar), as well as micropore % + 3×N% (nitrogen content) and the hysteresis width (bar). (The dashed line represents a linear relationship). Without incorporation of the N content, the relationship is rather scattered, as can be seen in Figure 7a. In Figure 7, the hysteresis width for G-800(H_2O), G-850-5(H_2O) and G-2.3-2(H_2O) is arbitrarily assigned as zero in order to better fit the importance of the N content in light of the CO_2 sorption performance of G-2.3-2(H_2O). Comparison of the linear fits before and after the inclusion of nitrogen content clearly reveal the importance of the nitrogen content in CO_2-hydrate formations in PCs (Figure 7). Better fit The hysteretic CO_2–sorption of the hydrated PCs points to stronger adsorption interaction between the CO_2 and the hydrated PCs. Therefore, smaller hysteresis width is required for fast kinetics of CO_2 sorption. Of all the studied hydrated PCs, uGilT(H_2O) has the smallest hysteresis width, along with micropore content of 73% and negligible N content. Thus, in order to achieve even smaller hysteresis width according to the linear relationship shown in Figure 7, we would suggest a PC with microporosity in the range of 73% - 90%. This suggestion is in accord with the mechanism proposed in this work, which is based on gas phase adsorption of CO_2 in micropores that are 'blocked in' by formation of CO_2–hydrates within the 'outer' meso- and macropores. Therefore, it is beneficial to have mixed micro- and mesopore distribution in PCs in order to achieve efficient CO_2-capture based on the CO_2-hydrate formation. Importantly, it is noteworthy that for conventional CO_2-hydrates, the $CO_2 \times nH_2O$ ratio, n is 5.72.[25-30] However, in our case, this ratio is considerably smaller (n = 1.8 and n = 2.8, depending on temperature).[42] Such a small ratio shows that PC(H_2O) samples adsorb much more CO_2 within the pores to an extent that is structurally impractical to form for conventional CO_2–hydrates.

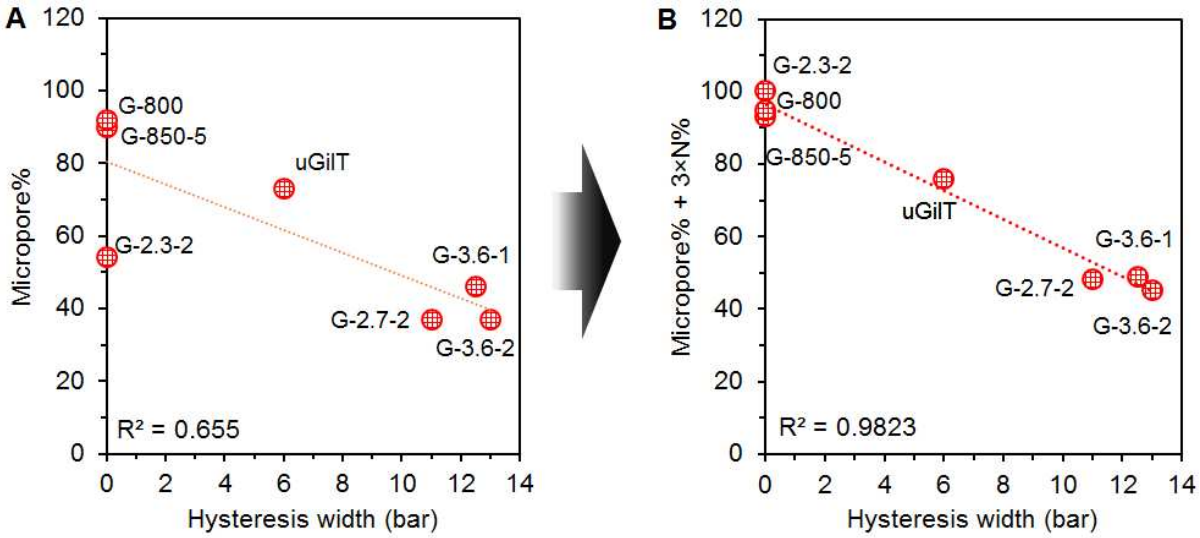

Figure 7. The diagram representing the direct comparison of the relationship between the CO_2-hydrate formation hysteresis width and the micropore percentage A) before and B) after the inclusion of nitrogen content percentage.

We have previously described the pressure and temperature dependence of the hysteretic CO_2 sorption isotherm and their relevance to the CO_2–hydrate formation process.[42] Here, we explore the relationship between pressure of the CO_2–hydrate formation (*i.e*. pressure at the beginning of the formation of hysteresis loop) and temperature in the range of 258-323 K so as to generate a phase-equilibrium diagram for CO_2–hydrate formation within uGilT(H_2O) as shown in Figure 8.[42] The pressure-temperature range of stability for CO_2–hydrate formation within uGilT(H_2O) was compared with the phase-diagrams of pure CO_2 gas-liquid transition, and pure CO_2–hydrate gas-solid and liquid-solid transitions (Figure 8).[51,52] As shown in Figure 8, the pressure for CO_2–hydrate formation equilibrium within uGilT(H_2O) significantly decreases above 280 K in comparison with pure aqueous CO_2–hydrate equilibrium pressure. This implies that the stability of CO_2–hydrate within uGilT(H_2O) is increased presumably *via* compensating the system

entropy within the porous media. Hence, the formation of smaller CO_2–hydrate crystals does not require stronger hydrogen-bonding within the porous media. Therefore, the proposed mechanism of CO_2 capture is in accord with the phase-diagram of CO_2–hydrate formation within uGilT(H_2O).

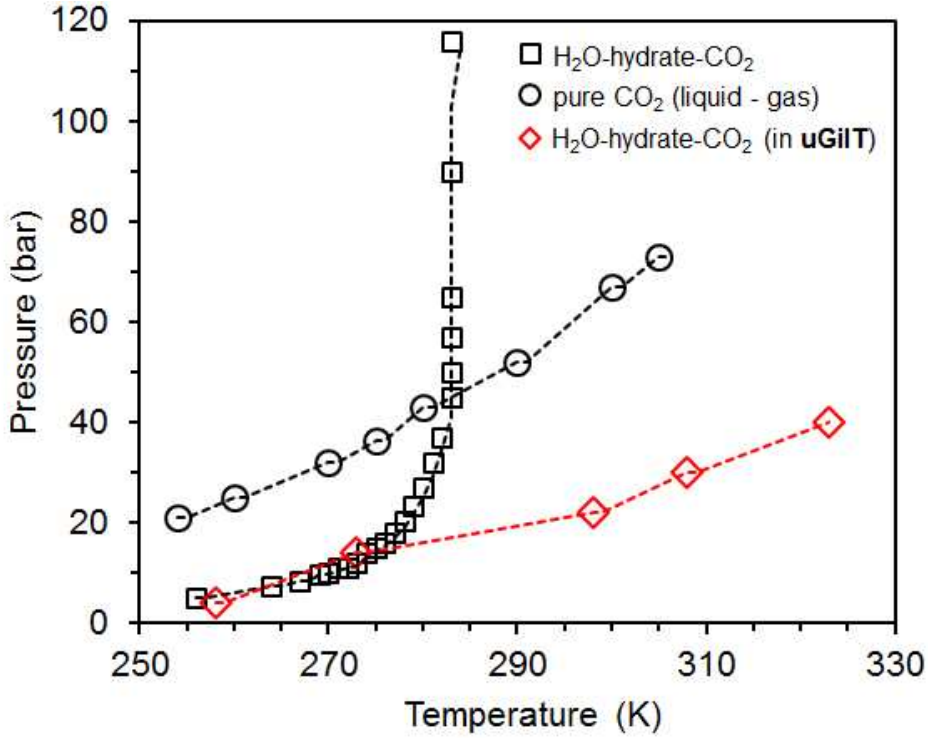

Figure 8. Phase equilibrium conditions of CO_2 hydrates, vapor-liquid phase equilibrium for pure CO_2 and phase equilibrium conditions of CO_2 hydrates within uGilT.

CONCLUSIONS

In summary, detailed analysis and characterization of the pore structure and surface functionalities of PCs, and their effect on CO_2–uptake performance in the presence (hydrated) or absence (dry) of water has revealed the importance of pore size and pore size distribution as well as the nitrogen content on the adsorption process. Supermicroporous carbon, with pores < 2 nm, show blocking of the pores with water that prevents hysteretic CO_2–hydrate formation thus limiting the overall

CO_2 uptake. Alternatively, mesoporous hydrated carbons show higher and more stable CO_2–hydrate formations that act to limit the CO_2–capture capacity to the specifics of the CO_2–hydrate structure. A high nitrogen content in the PCs acts to prevent the formation of CO_2-hydrates due to destabilization of the CO_2-hydrates arising from stronger noncovalent interactions between the nitrogen functional groups and H_2O or CO_2. Our findings provide additional understanding that is required for further development of CO_2–capture processes that are based on the gas-hydrate formations. Knowledge of the effects of pore structure and surface functionalities may allow the preparation of targeted materials or ready screening of porous materials for enhanced gas capture capacity and selectivity. In particular, materials with a mixed micro-and mesopore structure in combination with low nitrogen content, may provide very attractive CO_2–capture capacity and kinetics based on CO_2–hydrate formation.

EXPERIMENTAL SECTION

Untreated Gilsonite was provided by Prince Energy. All other chemicals were purchased from Millipor-Sigma and used without further purification unless otherwise stated.

Sample preparations. uGilT, G-800, G-850-5, G-2.3-2, G-2.7-2, G-3.6-1, and G-3.6-2 were prepared as previously reported.[9, 42-45] Briefly, uGilT was prepared by activation at 750 ºC of well-mixed Untreated Gilsonite with potassium hydroxide (potassium hydroxide/Untreated gilsonite weight ratio = 4).[42,45] G-800 and G-850-5 were prepared by activation at 800 ºC for 1 h and 850 ºC for 5 h, respectively, of α-D-glucose with potassium oxalate in 3.6 weight ratio of potassium oxalate/glucose.[9] G-2.3-2 and G-2.7-2 were prepared by activation at 800 ºC of α-D-glucose in the presence of melamine (glucose/melamine ratio = 2) with potassium oxalate in potassium oxalate/glucose ratio of 2.3 and 2.7, respectively. G-3.6-1, and G-3.6-2 were also prepared in

analogous way with differing glucose/melamine ratio = 3.6, and potassium oxalate/glucose ratio of 1 and 2, respectively.[9] Porous carbon samples were dried in oven at 150 ºC for 24 h at ambient pressure before use in their dry form. Preparation of hydrated PCs was done by submersing dry carbon samples in 5 mL nanopure water within a 20 mL vial, which was then put in a vacuum desiccator vessel under vacuum at 100 mTorr for 1 h until the bubbles from the samples stopped appearing. During this time, water is expected to enter into the pores, and water-imbibed porous carbon is obtained. Afterwards, the solid carbon material was filtered under vacuum at 30 Torr to yield precursor-wet samples (PC-H_2O) with a water to carbon weight ratio of ~2-3, although the powder surface appeared dry. PC-H_2O samples were dried at 110 ºC for 30 min to form the final water incorporated (hydrated) porous material PC(H_2O) with water to carbon weight ratio adjusted to 1.5.

Volumetric gas sorption. Volumetric sorption measurements of CO_2 were carried out in an automated Sievert instrument (Setaram PCTPro).[17] The sorbent was placed in a stainless steel sample cell, wherein dry samples were pretreated at 150 °C for 2 h under vacuum (~20 mTorr) and hydrated PC(H_2O) samples were pretreated at 25 °C for 5 min under vacuum. The sample volume was calibrated by helium before the sorption measurement. At each step of the measurement, testing gas was expanded from the reference reservoir into the sample cell until the system pressure reached equilibrium. The pressure transducer (Rosemount 3051S series) has a pressure range of 0-200 bar with an accuracy of < 1% of reading.

Gravimetric gas sorption. Gravimetric sorption measurements of CO_2 were carried out in a Rubotherm magnetic suspension balance (Rubotherm, Germany).[24,25] A blank test without sample was used to measure the weight and volume of the empty sample holder. For a typical measurement, the sorbent was placed in the sample holder, and dry samples were pretreated at 120

°C for 2 h under vacuum (~ 20 mTorr) and hydrated PC(H_2O) samples were pretreated at 25 °C for 5 min under vacuum. A buoyancy test with helium was then used to measure the sample weight and sample volume before the sorption measurement.

Characterization. The XPS analyses were obtained on a PHI Quantera SXM scanning X-ray microprobe system using a 100 µm X-ray beam with take-off angle of 45° and pass energy of 140 eV for the survey scan, and 26 eV for the high resolution elemental analysis. The surface areas, pore volumes and pore size distributions of different samples were obtained using an automated Micromeritics ASAP 2020 sorptometer *via* nitrogen physisorption at −196 °C. The dry samples were heated at 150 °C for 15 h for uGilT, and at 200 °C for 1 h for G-800 and G-850-5 under vacuum (20 mTorr) before each measurement. The apparent surface area (S_{BET}) was computed using appropriate relative pressure range data from nitrogen sorption isotherms using the Brunauer-Emmett-Teller (BET) method. The total pore volume (V_p) was determined from the amount of nitrogen adsorbed at $P/P_o \sim 0.95$, while the pore volume arising from micropores (V_m) was obtained by applying the Dubinin-Radushkevich equation (DR) or the Quenched-Solid Density Functional Theory (QSDFT). The pore size distributions (PSDs) were determined using the QSDFT applied to the nitrogen adsorption data assuming a slit pore model. Elemental composition (C, H, N and O) was determined using a LECO CHN-932 microanalyzer. The ATR-IR measurements conducted on a Fourier transform infrared spectrometer (Nicolet Nexus 670) equipped with an attenuated total reflectance system (Nicolet, Smart Golden Gate) and a MCT-A detector.

ACKNOWLEDGEMENTS

A. S. J. thanks the financial support by King Fahd University of Petroleum and Minerals for funding though project DSR SR171007. M. S. and A. B. F. thank funding by FICYT Regional Project (GRUPIN14-102) and Spanish MINECO-FEDER (CTQ2015-63552-R).

SUPPORTING INFORMATION

Additional X-ray photoelectron spectra and analysis of PCs. This material is available free of charge via the Internet at http://pubs.acs.org.

REFERENCES

1. Figueroa, J. D.; Fout, T.; Plasynski, S.; McIIvried, H.; Srivastava, R. D. Advances in CO_2 capture technology-The U.S. Department of Energy's Carbon Sequestration Program. *Int. J. Greenhouse Gas Control* **2008**, *2*, 9−20.
2. Yang, R. T. *Adsorbents: Fundamentals and Applications;* Wiley Interscience: Hoboken, NJ, 2003.
3. Zhang, X.Q.; Li, W.C.; Lu, A.H. Designed Porous Carbon Materials for Efficient CO_2 Adsorption and Separation. *New Carbon Mater*. **2015**, *30*, 481−501.
4. D'Alessandro, D. M.; Smit, B.; Long, J. R. Carbon Dioxide Capture: Prospects for New Materials. *Angew. Chem. Int. Ed.* **2010**, *49*, 6058–6082.
5. Choi, S.; Drese, J. H.; Jones. C. W. Adsorbent Materials for Carbon Dioxide Capture from Large Anthropogenic Point Sources. *ChemSusChem* **2009**, *2*, 796 – 854.
6. Ma, T.-Y.; Liu, L.; Yuan, Z.-Y. Direct Synthesis of Ordered Mesoporous Carbons. *Chem. Soc. Rev*. **2013**, 42, 3977−4003.
7. Presser, V.; McDonough, J.; Yeon, S. H.; Gogotsi, Y. Effect of Pore Size on Carbon Dioxide

Sorption by Carbide Derived Carbon. *Energy Environ. Sci*. **2011**, *4*, 3059−3066.

8. Presser, V.; Heon, M.; Gogotsi, Y. Carbide-Derived Carbons − from Porous Networks to Nanotubes and Graphene. *Adv. Funct. Mater*. **2011**, *21*, 810−833.
9. Sevilla, M.; Al-Jumialy, A. S. M.; Fuertes, A. B.; Mokaya, R. Optimization of the Pore Structure of Biomass-Based Carbons in Relation to Their Use for CO_2 Capture under Low- and High-Pressure Regimes. *ACS Appl. Mater. Interfaces* **2018**, *10*, 1623−1633.
10. Morris, R.E.; Wheatley, P.S. Gas Storage in Nanoporous Materials. *Angew. Chem. Int. Ed.* **2008**, *47*, 4966-4981.
11. Wickramaratne, N.P.; Jaroniec, M. Importance of Small Micropores in CO_2 Capture by Phenolic Resin-Based Activated Carbon Spheres. *J. Mater. Chem. A* **2013**, *1*, 112-116.
12. Nugent, P.; Belmabkhout, Y.; Burd, S. D.; Cairns, A. J.; Luebke, R.; Forrest, K.; Pham, T.; Ma, S. Q.; Space, B.; Wojtas, L.; Eddaoudi, M.; Zaworotko, M. J. Porous Materials with Optimal Adsorption Thermodynamics and Kinetics for CO_2 Separation. *Nature* **2013**, *495*, 80–84.
13. Chen, K.-J.; Madden, D. G.; Pham, T.; Forrest, K. A.; Kumar, A.; Yang, Q.-Y.; Xue, W.; Space, B.; Perry IV, J. J.; Zhang, J.-P.; Chen, X.-M.; Zaworotko, M. J. Tuning Pore Size in Square-Lattice Coordination Networks for Size-Selective Sieving of CO_2. *Angew. Chem. Int. Ed.* **2016**, *55*, 10268-10272.
14. Wang, J. T.; Chen, H. C.; Zhou, H. H.; Liu, X. J.; Qiao, W. M.; Long, D. H.; Ling, L. C. Carbon Dioxide Capture Using Polyethylenimine-Loaded Mesoporous Carbons. *J. Environ. Sci.* **2013**, *25*, 124−132.
15. Hwang, C. C.; Jin, Z.; Lu, W.; Sun, Z. Z.; Alemany, L. B.; Lomeda, J. R.; Tour, J. M. *In Situ* Synthesis of Polymer-Modified Mesoporous Carbon CMK-3 Composites for CO_2

Sequestration. *ACS Appl. Mater. Interfaces* **2011**, *3*, 4782−4786.

16. Wang, M.; Yao, L. W.; Wang, J. T.; Zhang, Z. X.; Qiao, W. M.; Long, D. H.; Ling, L. C. Adsorption and Regeneration Study of Polyethylenimine-Impregnated Millimeter-Sized Mesoporous Carbon Spheres for Post-Combustion CO_2 Capture. *Appl. Energy* **2016**, *168*, 282−290.
17. Jalilov, A. S.; Ruan, G.; Hwang, C. C.; Schipper, D. E.; Tour, J. J.; Li, Y.; Fei, H.; Samuel, E. L.; Tour, J. M. Asphalt-Derived High Surface Area Activated Porous Carbons for Carbon Dioxide Capture. *ACS Appl. Mater. Interfaces* **2015**, *7*, 1376−1382.
18. Sevilla, M.; Valle-Vigon, P.; Fuertes, A. B. N-Doped Polypyrrole-Based Porous Carbons for CO2 Capture. *Adv. Funct. Mater*. **2011**, *21*, 2781−2787.
19. Wang E.-J.; Sui Z.-Y.; Sun Y.-N.; Ma Z.; Han, B. H. Effect of Porosity Parameters and Surface Chemistry on Carbon Dioxide Adsorption in Sulfur-Doped Porous Carbons. *Langmuir* **2018**, *34*, 6358-6366.
20. Ghosh, S.; Barron, A. R. Optimizing Carbon Dioxide Uptake and Carbon Dioxide-Methane Selectivity of Oxygen-Doped Porous Carbon Prepared from Oxygen Containing Polymer Precursors. *ChemistrySelect* **2017**, *2*, 11959-11968.
21. Li, Z.; Ma, X.; Xiong, S.; Ye, Y.; Yao, Z.; Lin, Q.; Zhang, Z.; Xiang, S. Facile Synthesis of Oxidized Activated Carbons for High-Selectivity and Low-Enthalpy CO_2 Capture from Flue Gas. *New J. Chem*. **2018**, *42*, 4495-4500.
22. Zhang, Z.; Wang, H.; Chen, X.; Xie, R.; Gao, P.; Wei, W.; Sun, Y. CO_2 Sorption in Wet Ordered Mesoporous Silica Kit-6: Effects of Water Content and Mechanism on Enhanced Sorption Capacity. *Adsorption* **2014**, *20*, 883– 888.
23. Zhou, J.; Su, W.; Sun, Y.; Deng, S.; Wang, X. Enhanced CO_2 Sorption on Ordered Mesoporous

Carbon CMK-3 in the Presence of Water. *J. Chem. Eng. Data*, **2016**, *61*, 1348–1352.

24. Wang, Y.; Zhou, Y.; Liu, C.; Zhou, L. Comparative Studies of CO_2 and CH_4 Sorption on Activated Carbon in Presence of Water. *Colloids Surf. A* **2008**, *322*, 14–18.
25. Henriet, J.-P.; Mienert, J. *Gas Hydrates: Relevance to World Margin Stability and Climatic Change*; Geological Society of London Special Publication, 137, 1998.
26. Mandelcorn, L. Clathrates. *Chem. Rev*. **1959**, *59 (5)*, 827-839.
27. Englezos, P. Clathrate Hydrates. *Ind. Eng. Chem. Res*. **1993**, *32(7)*, 1251-1274.
28. Van der Waals, J. H.; Platteeuw, J. C. Clathrate Solutions. *Adv. Chem. Phys*. **1959**, *2*, 1-57.
29. Englezos, P.; Kalogerakis, N. E.; Bishnoi, P. R. Formation and Decomposition of Gas Hydrates of Natural Gas Components. *J. Inclusion Phenom. Mol. Recognit. Chem*. **1990**, *8*, 89-101.
30. Circone, S.; Stern, L. A.; Kirby, S. H.; Durham, W. B.; Chakoumakos, B. C.; Rawn, C. J.; Rondinone, A. J.; Ishii, Y. CO_2 Hydrate: Synthesis, Composition, Structure, Dissociation Behavior, and a Comparison to Structure I CH_4 Hydrate. *J. Phys. Chem. B*, **2003**, *107*, 5529–5539.
31. Babu, P.; Linga, P.; Kumar, R.; Englezos, P. A Review of the Hydrate Based Gas Separation (HBGS) Process for Carbon Dioxide Pre-Combustion Capture. *Energy* **2015**, 85, 261– 279.
32. Sloan, E. D. Jr. Fundamental Principles and Applications of Natural Gas Hydrates. *Nature*, **2003**, *426*, 353-359.
33. Englezos, P.; Lee, J.D. Gas Hydrates: A Cleaner Source of Energy and Opportunity for Innovative Technologies. *Korean J. Chem. Eng*. **2005**, *22*, 671-681.
34. Fan, S.; Yang, L.; Lang, X.; Wang, Y.; Xie D. Kinetics and Thermal Analysis of Methane Hydrate Formation in Aluminum Foam. *Chem. Eng. Sci*. **2012**, *82*, 185–193.
35. Sun, Y.; Xue, Q.; Zhou, Y.; Zhou, L. Sorption Equilibria of CO_2/CH_4 Mixture on Activated

Carbon in the Presence of Water. *J. Colloid Interface Sci*. **2008**, *322*, 22−26.

36. Sun, Y.; Wang, Y.; Zhang, Y.; Zhou, Y.; Zhou, L. CO_2 Sorption in Activated Carbon in the Presence of Water. *Chem. Phys. Lett*. **2007**, *437*, 14– 16.
37. Kang, S. P.; Lee, J.; Seo, Y. Pre-Combustion Capture of CO_2 by Gas Hydrate Formation in Silica Gel Pore Structure. *Chem. Eng. J*. **2013**, *218*, 126– 132.
38. Casco, M. E.; Rey, F..; Jordá, J. L.; Rudić, S.; Fauth, F.; Martínez-Escandell, M.; Rodríguez-Reinoso, F.; Ramos-Fernández, E. V.; Silvestre-Albero. J. Paving the Way for Methane Hydrate Formation on Metal–Organic Frameworks (MOFs). *Chem. Sci.*, **2016**, *7*, 3658-3666.
39. Soubeyrand-Lenoir, E.; Vagner, C.; Yoon, J.W.; Bazin, P.; Ragon, F.; Hwang, Y. K.; Serre, C.; Chang, J.-S.; Llewellyn, P. L. How Water Fosters a Remarkable 5-Fold Increase in Low-Pressure CO2 Uptake Within Mesoporous MIL-100(Fe). *J. Am. Chem. Soc*. **2012**, *134*, 10174 – 10181.
40. Sloan, E. D. Jr.; Koh, C. A. *Clathrate Hydrates of Natural Gases*; Boca Raton, Florida, USA: Chemical Industries, CRC Press, 119, 2008.
41. Ripmeester, J. A.; Tse, J. S.; Ratcliffe, C. I.; Powell, B. M. A New Clathrate Hydrate Structure. *Nature*, **1987**, *325*, 135-139.
42. Jalilov, A. S.; Li, Y.; Kittrell, C.; Tour. J. M. Increased CO_2 Selectivity of Asphalt-Derived Porous Carbon Through Introduction of Water into Pore Space. *Nat. Energy* **2017**, *2*, 932-939.
43. Sevilla, M.; Sangchoom, W.; Balahmar, N.; Fuertes, A. B.; Mokaya R. Highly Porous Renewable Carbons for Enhanced Storage of Energy-Related Gases (H_2 and CO_2) at High Pressures. *ACS Sustainable. Chem. Eng.* **2016**, *4*, 4710-4716.
44. Cox, M.; Mokaya, R. Ultra-High Surface Area Mesoporous Carbons for Colossal Pre Combustion CO_2 Capture and Storage as Materials for Hydrogen Purification. *Sustainable*

Energy Fuels **2017**, *1*, 1414-1422.

45. Jalilov, A. S.; Li, Y.; Tian, J.; Tour, J. M. Ultra-High Surface Area Activated Porous Asphalt for CO_2 Capture through Competitive Adsorption at High Pressures. *Adv. Energy Mater*. **2017**, *7*, No. 201600693.
46. Weidenthaler. C. Pitfalls in the Characterization of Nanoporous and Nanosized Materials. *Nanoscale*, **2011**, *3*, 792–810.
47. Li, Y.; Luong, D. X.; Zhang, J.; Tarkunde, Y. R.; Kittrell, C.; Sargunaraj, F.; Ji, Y.; Arnusch, C. J.; Tour, J. M. Laser-Induced Graphene in Controlled Atmospheres: From Superhydrophilic to Superhydrophobic Surfaces, *Adv. Mater*. **2017**, *29*, No. 1700496.
48. Zhou, Y.; Dai, M.; Zhou, L.; Sun, Y.; Su, W. Storage of Methane on Wet Activated Carbon: Influence of Pore Size Distribution, *Carbon* **2004**, *42*, 1855–1858.
49. Cox, S. J.; Taylor, D. J. F.; Youngs, T. G. A.; Soper, A. K.; Totton, T. S.; Chapman, R. G.; Arjmandi, M.; Hodges, M. G.; Skipper, N. T.; Michaelides, A. Formation of methane hydrate in the presence of natural and synthetic nanoparticles. *J. Am. Chem. Soc*. **2018**, *140*, 3277–3284.
50. Liu, J.; Wei, Y.; Meng, W.; Li, P.-Z.; Zhao, Y.; Zou, R. Understanding the Pathway of Gas Hydrate Formation with Porous Materials for Enhanced Gas Separation, *Research* **2019**, *2019*, No. 3206024.
51. Kang, S. P.; Lee, H.; Lee, C. S.; Sung, W. M. Hydrate Phase Equilibria of the Guest Mixtures Containing CO_2, N_2, and Tetrahydrofuran. *Fluid Phase Equil*. **2001**, *185*, 101-109.
52. Yuan Q.; Sun, C.-Y.; Liu, B.; Wang, X.; Ma, Z.-W.; Ma, Q.-L.; Yan, L.-Y.; Chen, G.-J.; Li, Q.-P.; Li S.; Zhang K. Methane Recovery from Natural Gas Hydrate in Porous Sediment Using Pressurized Liquid CO_2. *Energy Convers. Manage*. **2013**, *67*, 257-264.

Graphical Abstract